UNCLASSIFIED
SECURITY CLASSIFICATION OF THIS PAGE

MASTER COPY FILE COPY FOR REPRODUCTION PURPOSES (2)

ITATION PAGE Proposal No. 24453-PH

1a. REPORT SECURITY CL: Unclassifi	RESTRICTIVE MARKINGS
2a. SECURITY CLASSIFICA	DISTRIBUTION/AVAILABILITY OF REPORT
2b. DECLASSIFICATION/D	Approved for public release; distribution unlimited.
4. PERFORMING ORGANIZATION REPORT NUMBER(S)	5. MONITORING ORGANIZATION REPORT NUMBER(S): ARO 24453.7-PH
6a. NAME OF PERFORMING ORGANIZATION: DUKE UNIVERSITY	6b. OFFICE SYMBOL (If applicable): n/a
7a. NAME OF MONITORING ORGANIZATION: U. S. Army Research Office	
6c. ADDRESS (City, State, and ZIP Code): Dr. Frank C. De Lucia, Department of Physics, Duke University, Durham, NC 27706	7b. ADDRESS (City, State, and ZIP Code): P. O. Box 12211, Research Triangle Park, NC 27709-2211
8a. NAME OF FUNDING/SPONSORING ORGANIZATION: U. S. Army Research Office	8b. OFFICE SYMBOL (If applicable)
9. PROCUREMENT INSTRUMENT IDENTIFICATION NUMBER: DAAL03-86-K-0147	
8c. ADDRESS (City, State, and ZIP Code): P. O. Box 12211, Research Triangle Park, NC 27709-2211	10. SOURCE OF FUNDING NUMBERS

PROGRAM ELEMENT NO.	PROJECT NO.	TASK NO.	WORK UNIT ACCESSION NO.

11. TITLE (Include Security Classification): Spectroscopic Investigations of Nonambient Systems with Millimeter and Submillimeter Probes

12. PERSONAL AUTHOR(S): Dr. Frank C. De Lucia

13a. TYPE OF REPORT	13b. TIME COVERED	14. DATE OF REPORT (Year, Month, Day)	15. PAGE COUNT
FINAL	FROM 1/8/86 TO 1/2/90	June 28, 1990	33 pages

16. SUPPLEMENTARY NOTATION: The view, opinions and/or findings contained in this report are those of the author(s) and should not be construed as an official Department of the Army position, policy, or decision, unless so designated by other documentation.

17. COSATI CODES			18. SUBJECT TERMS (Continue on reverse if necessary and identify by block number)
FIELD	GROUP	SUB-GROUP	

19. ABSTRACT (Continue on reverse if necessary and identify by block number)

The project, "Spectroscopic Investigations of Nonambient Systems with Millimeter and Submillimeter Probes," addressed a broad range of scientific topics and technological developments important to this spectral region. For the purposes of this discussion, we have divided the report on research results into three parts: (1) Energy transfer in polyatomic molecules, especially those of importance in far infrared lasers; (2) Molecular collisional processes at very low temperature (5 K), and (3) Development and uses of millimeter and submillimeter technology. Also included is a list of personnel who worked on these projects.

This project addressed the development and use of spectroscopic techniques for the study of molecular systems under nonambient conditions. Emphasis was placed on the use of millimeter and submillimeter spectroscopic methods as diagnostic probes of these environments although many of these techniques are also applicable in other spectral regions. In some cases, the mm/submm spectral region was especially advantageous for the work while in others it was merely convenient because of our experience and equipment base in this part of the spectrum. (jhd)

20. DISTRIBUTION/AVAILABILITY OF ABSTRACT	21. ABSTRACT SECURITY CLASSIFICATION
☐ UNCLASSIFIED/UNLIMITED ☒ SAME AS RPT. ☐ DTIC USERS	Unclassified

22a. NAME OF RESPONSIBLE INDIVIDUAL	22b. TELEPHONE (Include Area Code)	22c. OFFICE SYMBOL

DD FORM 1473, 84 MAR — 83 APR edition may be used until exhausted. All other editions are obsolete.

SECURITY CLASSIFICATION OF THIS PAGE
UNCLASSIFIED

SPECTROSCOPIC INVESTIGATIONS OF NONAMBIENT SYSTEMS WITH MILLIMETER AND SUBMILLIMETER PROBES

FINAL REPORT

Frank C. De Lucia

June 30, 1990

U. S. Army Research Office

DAAL03-86-K-0147

Duke University

TABLE OF CONTENTS

ABSTRACT OF WORK UNDER ARO CONTRACT DAAL03-86-K-0147

The project, "Spectroscopic Investigations of nonambient systems with Millimeter and Submillimeter Probes," addressed a broad range of scientific topics and technological developments important to this spectral region. For the purposes of this discussion, we have divided the report on research results into three parts: (1) Energy transfer in polyatomic molecules, especially those of importance in far infrared lasers; (2) Molecular collisional processes at very low temperature (< 5 K), and (3) Development and uses of millimeter and submillimeter technology. Also included is a list of personnel who worked on these projects.

I. INTRODUCTION AND BACKGROUND

This project addressed the development and use of spectroscopic techniques for the study of molecular systems under nonambient conditions. Emphasis was placed on the use of millimeter and submillimeter spectroscopic methods as diagnostic probes of these environments although many of these techniques are also applicable in other spectral regions. In some cases, the mm/submm spectral region was especially advantageous for the work while in others it was merely convenient because of our experience and equipment base in this part of the spectrum.

Much of what is proposed is based upon previous developments in our laboratory. In this Introduction, we will briefly discuss some of the basis for this work; in later sections more of the details and references are provided.

A. The mm/submm Spectral Region

1. The spectroscopic technique: The mm/submm spectroscopic technique which was used in many of these experiments has been developed over a period of years.[1-3] Briefly, the nonlinear harmonic generators which produce the mm/submm radiation are driven by klystrons or traveling wave tube amplifiers[4] in the region around 50 GHz. These microwave sources are in turn referenced to or driven by sources which are controlled by frequency synthesizers, effectively giving a synthesized source which is conveniently and continuously tunable throughout the region between ~ 100 - 1000 GHz. This mm/submm energy is radiated quasi-optically through the atomic and molecular system being studied and detected by an InSb detector operating at 1.5 K or a 0.3 K germanium bolometer. Associated electronics are used for frequency measurement and signal recovery. Systems of this type have proven to be reliable, easy to operate, and reasonably inexpensive. Because of these

attributes, a number of similar systems have now been built at laboratories around the world and have become the standard for a wide range of molecular studies in this spectral region.

2. Characteristics of mm/submm spectroscopy: Much of the work discussed in this report depended upon several important attributes of our technique for spectroscopic studies in the mm/submm spectral region. Among these are:

a) It is a very sensitive technique. Under equilibrium conditions, rotational absorption coefficients increase as $\nu^2 \rightarrow \nu^3$ and peak typically in the vicinity of 1000 GHz. Under optimum non-equilibrium conditions, achievable in our pumped experiments, concentrations as small as 100 cm^{-3} ($\sim 10^{-14}$ Torr partial pressure) can be studied with modest signal averaging. Calculations based on a more aggressive set of assumptions yield concentrations as small as 1 cm^{-3}.

b) Because of the broad tunable coverage in the frequency regime that corresponds to many of the rotational transitions of the small, fundamental species that we wish to study, transitions can be chosen on the basis of their diagnostic value rather than to satisfy coincidence criteria. Furthermore, because of the high resolution, spectral overlap is very rare.

c) It is an absorption technique. Because the transitions that are observed are rotational transitions with accurately known transition moments, the absolute absorption data can be accurately converted into molecular information.

d) Because we directly observe rotational transitions, the method is especially sensitive to rotational nonequilibria. For example, at 300 K and 300 GHz a 5 % change in the population of one of the states involved in a transition produces a 100 % change in the observed line strength.

e) Because this is the frequency regime in which a very large number of optically pumped lasers have been discovered, we can take advantage of the hundreds of man years that have been spent searching for CO_2 laser pump coincidences.

B. Applications

Over a number of years we have used these mm/submm techniques for a wide variety of spectroscopic investigations. In the sections below some of those that are related to the reported work are briefly discussed.

1. Spectroscopy of small, fundamental molecular species: The principal initial application of this spectroscopic technique was its use to develop a basic spectroscopic understanding of small, fundamental molecules in the mm/submm. Particular emphasis was placed on species of atmospheric, astronomical, chemical, and spectroscopic interest. This work has included studies of light asymmetric rotors such as H_2O and H_2S, prototype internal rotors such as HOOH and CH_3OH, light asymmetric rotors with electronic angular momenta such as NO_2, HO_2, and HCO, and a number of unstable species and ions such as CCH, NO^+, and LiH. In addition to the experimental aspects of this work, we have also developed theoretical and computational methods for characterizing to microwave accuracy these spectra over wide spectral ranges. Many (if not most) of these studies were the first to provide spectral characterization of these species to microwave accuracy over large portions of their rotational spectra in the mm/submm. This work is of importance to the reported work because the basic spectroscopic properties (energy levels, transition frequencies, transition moments, etc.) of the molecular species which we studied must first be well understood.

2. Collisionally cooled spectroscopy at very low temperatures: As is discussed in more detail in Section III, we have devoted a significant portion of our effort recently toward the development and exploitation of a collisional cooling technique which provides a simple method for the study of gas phase processes at temperatures below 5 K.[5,6] The scientific motivation for this work has been the desire to study molecular interactions in the regime where $kT \leq h\nu_r$. To this point we have focused our attention on the study of pressure broadening in the region between 5 K and 1.5 K and on investigations of vibrational and rotational relaxation at 77 K. In this regime we have found that the mechanisms responsible for broadening make a transition from being dominated by classical inelastic collisions at higher temperatures to a lower energy regime in which resonances associated with quasi-bound states become important. The variety and richness of the results that we have obtained have been beyond our expectations.

3. Collisional energy transfer: We have also done considerable work on the internal mechanisms of molecular lasers and the basic collisional energy transfer processes that are the basis of them, especially optically pumped FIR lasers.[7,8] Our emphasis has been on rotational processes both because this degree of freedom corresponds most closely with mm/submm devices and because a number of interesting basic problems exist in rotational energy transfer.

II. EXPERIMENTAL AND THEORETICAL CONSIDERATIONS

Because the thrust of this report is the study of molecular systems under nonambient conditions, it is useful to briefly consider the spectroscopic consequences of significant changes in temperature both on spectroscopic parameters and the physics of the systems being studied.

A. Gas Phase Molecular Interactions as a Function of Temperature

First consider the temperature scaling laws for the interaction of gas phase molecular systems and mm/submm radiation. For the purposes of numerical comparison, we will assume that a system originally at 300 K is cooled to 4 K and that it may be diluted in a collisional cooling gas.

1. Linewidth: In the mm/submm spectral region experiments are typically run under doppler broadened limits. Since doppler broadening is proportional to $T^{1/2}$, linewidths at 4 K are typically an order of magnitude narrower and correspondingly greater resolution and measurement accuracy are possible. In addition, since sensitivity is ordinarily determined by peak, not integrated intensity, this factor under many circumstances also adds an order of magnitude to system sensitivity. We have confirmed this expectation in a number of studies.[5,6,9-13]

2. Sensitivity: Several temperature dependent factors affect molecular absorption coefficients. The rotational absorption coefficient is given by

$$\alpha = [8\pi^2\nu/3ch] \cdot |\langle m|\mu|n\rangle|^2 \cdot [N/\Delta\nu] \cdot [1-e^{-h\nu/kT}] \cdot [1/Q_r]$$

where it has been factored to separate the individual temperature dependent terms. The behavior of $N/\Delta\nu$ depends upon the details of the pressure broadening, but simple theory gives

$$N/\Delta\nu \propto T^{-1/2}$$

Q_r is the rotational partition function which approaches 1 in the low temperature limit. If we consider molecules whose $J = 0 - 1$ transitions fall at ~ 100 GHz, Q_r is ~ 100 - 1000. The term $[1-e^{-h\nu/kT}]$, which represents the difference between induced absorption and emission varies between unity in the limit $h\nu >> kT$ and ~1/100 for transitions of ν ~ 100 GHz at 300 K. Together these factors represent a four or five order of magnitude gain in absorption coefficient for systems as very low temperature. Other factors are more dependent on the details

of the system. The dilution ratio of the spectroscopic gas in the cooling gas will reduce this gain for stable species, but the reduced pressure broadening parameters associated with zero dipole moment collision partners and the gains in detector sensitivity for low background environments will add to the overall system gains. The latter factor will be especially significant when detector noise is the limiting factor in the system. To give two typical examples, the absorption coefficients of gas phase CO and HCN at 4 K are 25 cm^{-1} and 10000 cm^{-1} respectively. Thus, we conclude that even at very large dilutions of the spectroscopic species in the collisional cooling gas, absorption coefficients will be very large. Again, this expectation has been confirmed in our recent work and molecules with small dilution ratios (~ 10^{-4} - 10^{-6}) are easily observable on an oscilloscope screen in real time.

3. Physics: The spectral complexity of many systems is considerably reduced at low temperature. For example, it has been elegantly demonstrated by many workers using free jet expansions that the complexity of rotational structure in room temperature spectra can be dramatically simplified.[14,15] In addition, rotational collisional processes are of both fundamental and practical importance and many articles and reviews on the subject have been written. In a review article, Brunner and Pritchard[16] compare and contrast 'photon' spectroscopy and 'collisional' spectroscopy. They point out that both spectroscopies are characterized (in principle) by massive amounts of data (mostly redundant) that should be calculable from a relatively small number of 'spectroscopic' constants. However, the nature of 'collisional' spectroscopy is such that it is much more difficult to invert the problem so that fundamental parameters may be recovered from the experimental results. Even if these parameters are given, it is usually a formidable computational task to calculate the effects of these collisions either for the comparison of experiment and theory or for use in other problems. This is because of the participation of the very large number of thermally accessible rotational states in each collision process and because of the increased complexity of molecule-molecule/atom interactions in comparison with molecule-field interactions. The dynamics of the interplay between theory and experiment are further hindered by the nature of the available experimental data. Fundamental parameters are recoverable from most experimental data only via complex (and usually unrealizable) deconvolutions. The origin of this difficulty is very similar to the cause of the theoretical complexity, the large number of thermally populated states and the nature of the molecular interaction. Thus, it is concluded that the very large reduction in the number of thermally populated states at low temperature will make the relation between observables and the fundamental interactions substantially more direct. This is one of the principal motivations for our work. Finally, these very low temperatures significantly enhance the production and lifetime of weakly bound complexes such as van der Waals molecules and also provide additional opportunities for the study of

ions and other transient species.

B. System Sensitivity as a Function of Temperature

Over much of the mm/submm spectral region, the sensitivity of our experimental technique is directly proportional to the sensitivity of the detector employed. The cooled detectors used in our work approach being ideal detectors in that their NEP's approach being limited by the fluctuations in the blackbody radiation that is incident on them along with the spectrometer signal. In fact, if one of these detectors is completely broadband and can view the entire 300 K blackbody spectrum, its NEP is limited to about 5×10^{-11} W/Hz$^{1/2}$. In the mm/submm the use of cooled filters that only pass the long wavelength portion of the 300 K blackbody along with the spectrometer signal can significantly improve this, and for a cutoff frequency of ν_m the NEP for an ideal broadband detector is given in the long wavelength limit by $NEP \sim kT\nu_m^{1/2}$.[17] For a ν_m = 1000 GHz, this correspond to ~ 10^{-15} W. The 1.5 K InSb detectors that we have used in these systems for many years[2] have NEP's in the range of 10^{-12} - 10^{-13} W/Hz$^{1/2}$ and the 0.3 K ^{3}He detector mentioned above has a NEP of the order 5×10^{-15} W/Hz$^{1/2}$, about 20 times better. It is our experience that this has added a similar amount to our system performance. However, the equation above shows that the construction of a more sensitive broadband detector for the mm/submm spectral region is not possible *if it must view a room temperature experiment.*

There has developed a substantial interest in the use of the mm/submm for astronomical applications. Because the noise limit is this case is often the 3 K blackbody background, there has been a considerable effort directed at developing detectors for this low background environment by the use of very low temperature techniques. This work has produced detectors whose NEP's are of the order of ~10^{-17} W/Hz$^{1/2}$. This is several orders of magnitude better than the limit set by the thermal background for detectors viewing the long wavelength tail of the blackbody distribution and about four orders of magnitude better than the 1.5 K detectors commonly used. We are in the initial stages of testing a similar system which is based on an adiabatic demagnetization refrigerator. Since much of the proposed work will take place in an ~4 K environment, we expect to be able to realize much of this advantage.

III. RESULTS

A. Pressure Broadening below 5 K via Collisional Cooling

1. Experimental results: To date we have investigated the helium pressure broadening characteristics as a function of temperature for a number of species including CO, NO, CH_3F, H_2S, DCl, HDO, OCS, and CH_2F_2 in the temperature region below 5 K.[5,6,9,10,11,12,13] These measurements have been made with the collisional cooling technique which we have described in the aforementioned papers. The expectation (based on the calculations of sensitivity, linewidth, etc. shown above) that the collisionally cooled technique should be generally applicable has thus been borne out. The only 'failures' that we have encountered have been traceable to injector designs that allowed condensation or freezing for some of the less volatile of the spectroscopic gases. Newer designs have completely eliminated this problem except for HDO, a case where we still have a problem providing smooth control of the flow rate.

Our development of the collisional cooling technique was motivated by both the general ideas discussed above as well as a desire to carry out specific experimental investigations. In general, we wanted to be able to experimentally investigate a regime for which $h\nu \leq kT$ in the microwave spectral region; thus having molecular systems in analogy to atoms at room temperature, with the energy level spacing large compared to kT. However, only part of the analogy between molecules at very low temperature and atoms under ambient conditions holds because at very low temperatures the collision energies are small or comparable to van der Waals binding energies. Thus, the molecular systems have the additional features of systems that can form quasibound states at very low temperature.[18-20] As a consequence, a rich spectrum of results has been observed that is dependent both on the molecular species and rotational state.

Before showing experimental results, it is worthwhile discussing some of the qualitative features that should be expected. Although it is always dangerous to ascribe too physical a picture to processes that are inherently nonclassical, doing so provides in this case a good mechanism for classifying and understanding the results of our experiments.

In the simplest picture of molecular collisions and their contributions to line broadening, the energy defect (which is a measure of the energy that is transferred between internal and external degrees of freedom) and its relation to kT plays an important role. Whenever this defect becomes too large, the efficiency of the collisions in producing broadening and/or inelastic collisions is reduced; and, in the limit of zero translational energy, this efficiency also becomes zero. However, an additional effect can become important in very low energy collisions. Because of the existence of shallow attractive wells in the intermolecular potential,

resonances in both the pressure broadening and inelastic cross sections associated with quasi-bound states can exist. Open channels with significant strength result from the contributions from rotational levels which lie at low enough energy to interact with the shallow wells.

Thus, in the limit of small collision energy there are two countervailing effects; the reduction in cross section due to the growth in the energy defect and the increase in cross section due to the low energy resonances. Because both of these effects are sensitive functions of the intermolecular potential and the energy level structure of the molecule, a wide variety of functional dependencies of cross section on temperature are observed. These qualitative expectations have been borne out by diagnostic calculations of Palma and Green for the CO - He system[21] and by the experimental results described below.

These ideas lead to the expectation that the pressure broadening cross sections of species with the most widely spaced energy levels should have the fewest resonances in their cross sections and the most rapid fall off in cross section because of large energy gaps. As shown in Fig. III.A.1, NO, DCl and H_2S all exhibit monotonically decreasing cross sections with decreasing temperature. However, even in these simplest cases the results are far from 'geometric': the cross section at 4.3 K for NO is modestly above its 300 K value of ~22 Å^2, for DCl very near its 300 K value of ~ 10 Å^2, but for H_2S much below its 300 K value of ~ 25 Å^2. In a contrasting example, shown in Fig. III.A.2, CH_3F (with its much more closely spaced energy levels) has a cross section at 4 K that is sub-

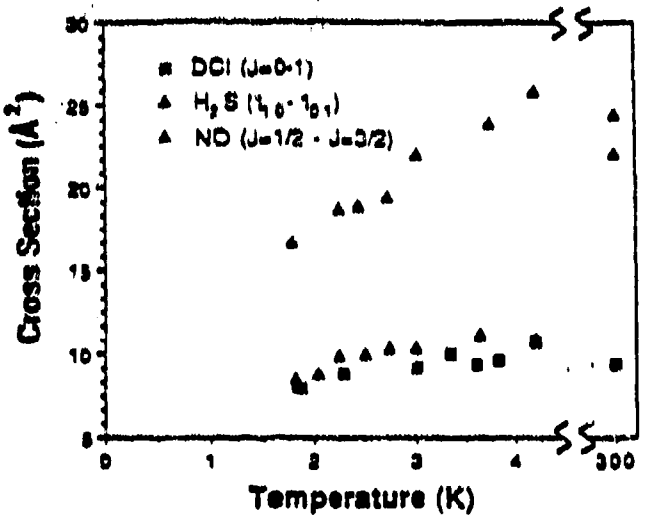

Figure III.A.1 Helium pressure broadening cross sections of NO, DCl, and H_2S below 5 K.

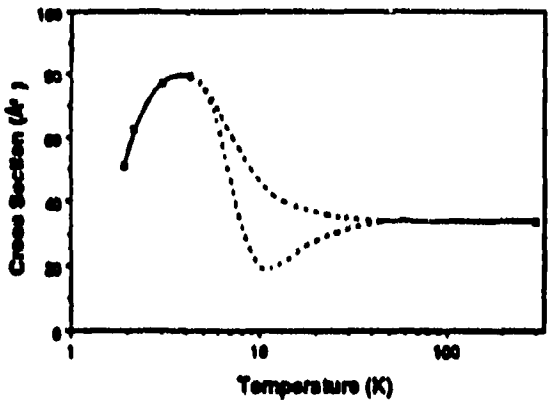

Figure III.A.2 Helium pressure broadening cross sections for the K = 0 component of the J = 2 - 3 transition of CH_3F. The dotted lines indicate possible connections between the classical region at high temperature and the cross sections below 5 K.

stantially higher than its room temperature value. The broken line in the figure is drawn to indicate the uncertainties associated with how the 300 K measurement connects with our results below 5 K. We have also observed about a 25% variation among different transitions at 4 K in CH_3F. It is useful to note that although CH_3F (and other species with fairly dense energy level structures) show cross sections at 4 K that are significantly higher than their 300 K values, all species observed to date show either flat or decreasing cross sections at T ~ 1.8 K.

Figure III.A.3 shows a comparison between the cross sections for the lowest rotational transitions of NO (J = 1/2 - 3/2) and CO (J = 0 - 1). As would be expected for these similar molecules, the cross sections at room temperature are essentially identical.[12,22] In addition, for CO measurements down to 77 K reveal an essentially unchanged cross section. However, at 4.2 K the results begin to rapidly diverge, with the NO cross section rapidly decreasing and the CO increasing.

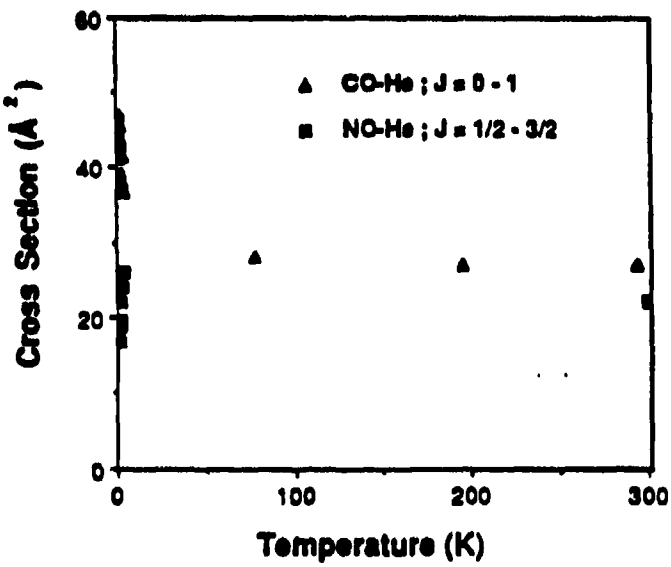

Figure III.A.3 A comparison of the helium pressure broadening cross sections for the lowest rotational transitions of CO and NO.

Figure III.A.4 shows the variation with J of the cross sections of CO for the region below 5 K. Inspection of this figure shows significant state to state variation in cross section,

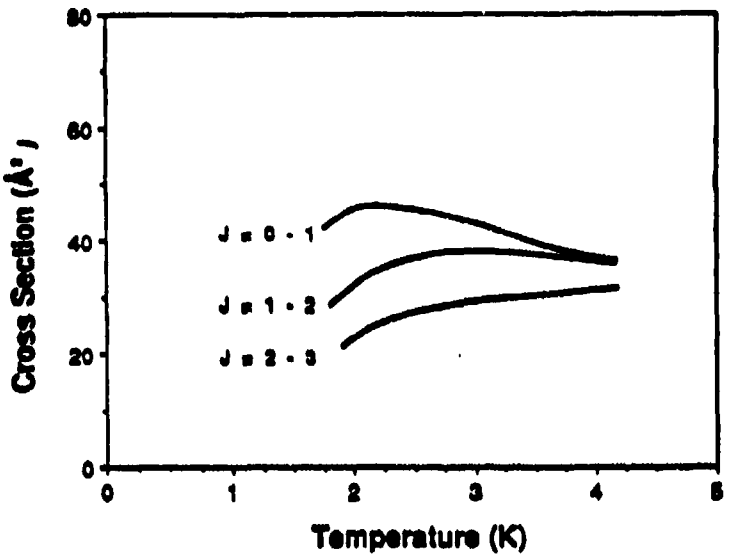

Figure III.A.4 The dependence on J of the cross section of CO below 5 K. The smooth lines are representations of the experimental data.

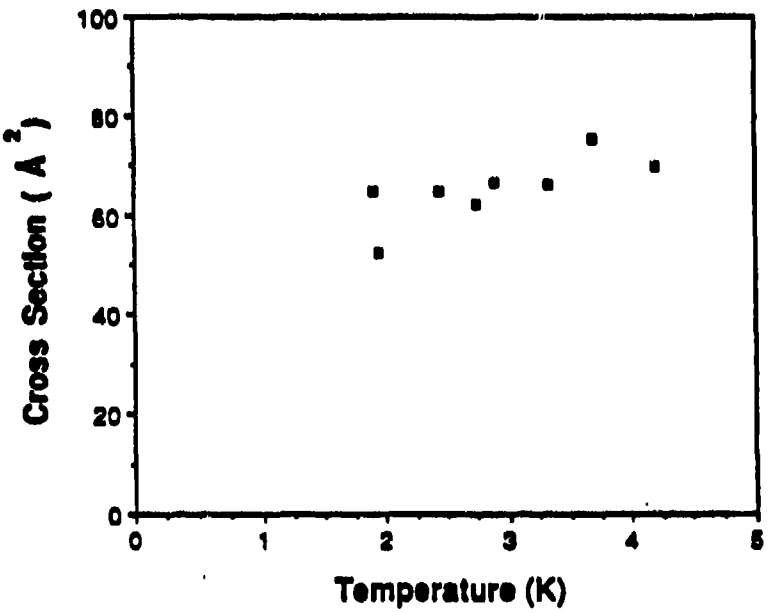

Figure III.A.5 Helium pressure broadening cross section for the 3_{22} - 3_{13} transition of CH_2F_2 below 5 K.

with the expected qualitative behavior, a faster decrease in cross section for the more widely spaced levels.

Recently, we have also studied the $3_{22} - 3_{13}$ transition of CH_2F_2 and the results are shown in Fig. III.A.5. In addition to this being the first asymmetric rotor with a reasonable dense energy level structure that we have studied, it contains the lower pump level for the well known CH_2F_2 FIR laser. Because this level is still significantly populated at 4 K, this system is an good candidate for time resolved rotational energy transfer studies at very low temperatures. This will be discussed in more detail in Section IV.

2. Discussion: Numerous calculations have shown that cross sections are especially sensitive to the intermolecular potential at low temperatures.[18, 19,20,21,23] Because these resonances require the existence of at least a shallow attractive well, the depth of the assumed well becomes critical. Only for the CO - He system have detailed calculations been published.[24] The results of these calculations for the J = 0 – 1 and J = 1 – 2 transitions are shown in Fig. III.A.6. Comparison of Figs. III.A.4 and III.A.6 shows basic agreement between the

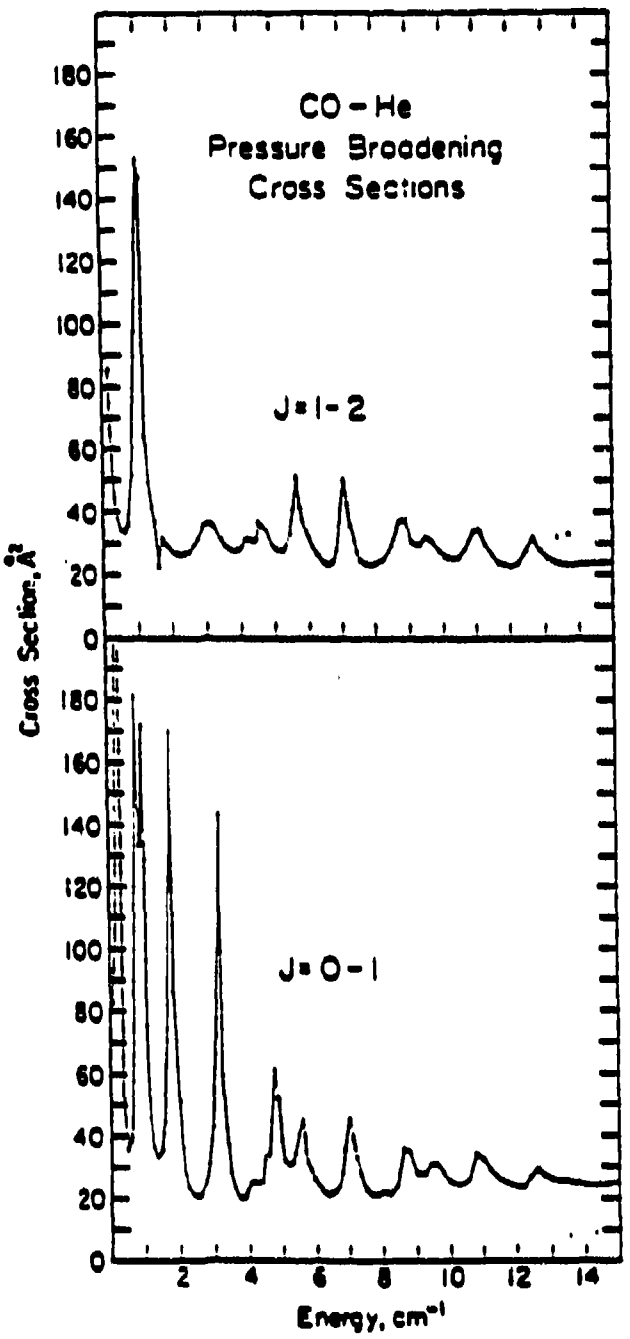

Figure III.A.6 Calculated helium pressure broadening cross section for the J = 0 - 1 and J = 1 - 2 transitions of CO.

experimental and theoretical results around 4 K, but at lower temperatures there are significant differences. The general theoretical prediction that the J = 1 – 2 cross section is smaller than the J = 0 – 1 is borne out, but for both transitions near 1.8 K the experimental values fall about 30% below the predictions of theory. It is thought that this is a result of the proclivity of the methods used to calculate the intermolecular potential to overestimate the depth of the attractive well.[25]

For CO - He the rapid rise in the calculated cross sections with reduced temperature results from the thermal average over a number of strong, sharp resonances in the cross section at low energy. These resonances are strongly dependent on the details of the assumed potential, and Palma and Green[21] have investigated this dependence in a subsequent paper. They calculated two additional sets of cross sections in which the depth of the attractive well of the CO - He potential used in the earlier work[24] was first reduced by one half and finally completely eliminated. The results of these calculations are shown in Fig. III.A.7. The most important result was the demonstration that a reduction in the attractive well reduces the number, width,

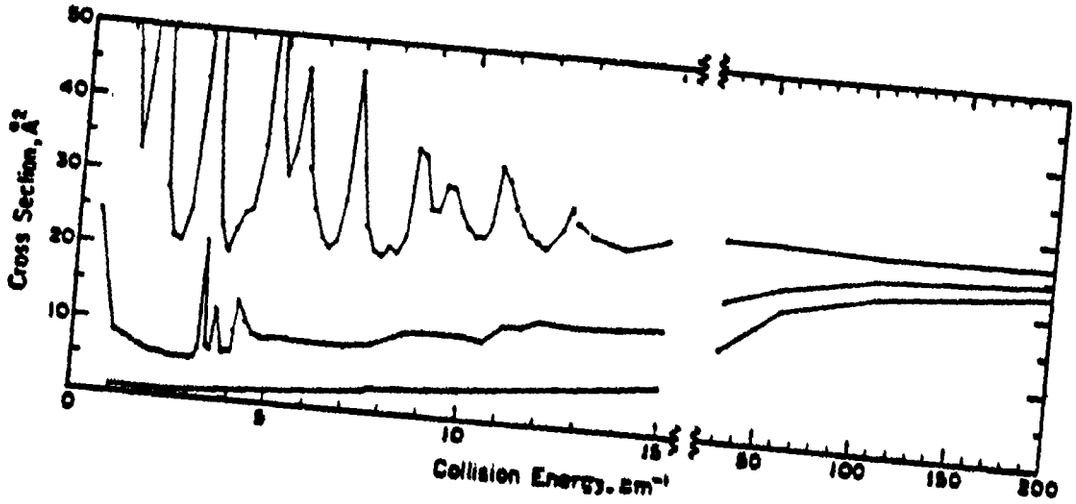

Figure II.A.7 Theoretical pressure broadening cross sections for the $J = 0 - 1$ line of CO. The upper curve is calculated from the normal potential. For the middle curve, the potential was modified by reducing the attractive part by half. For the bottom curve, the attractive part of the potential was eliminated.

and strength of the resonances; with a corresponding reduction in cross section. In fact, in the extreme of eliminating the well, the cross sections went to zero at 0 K, in satisfying agreement with physical intuition.

Recently, close coupled calculations similar to those discussed for CO - He have been done for the HDO - He system.[25] Figure III.A.8 shows the calculated pressure broadening cross section below 20 cm^{-1} for three HDO transitions. Prominent in these figures is the

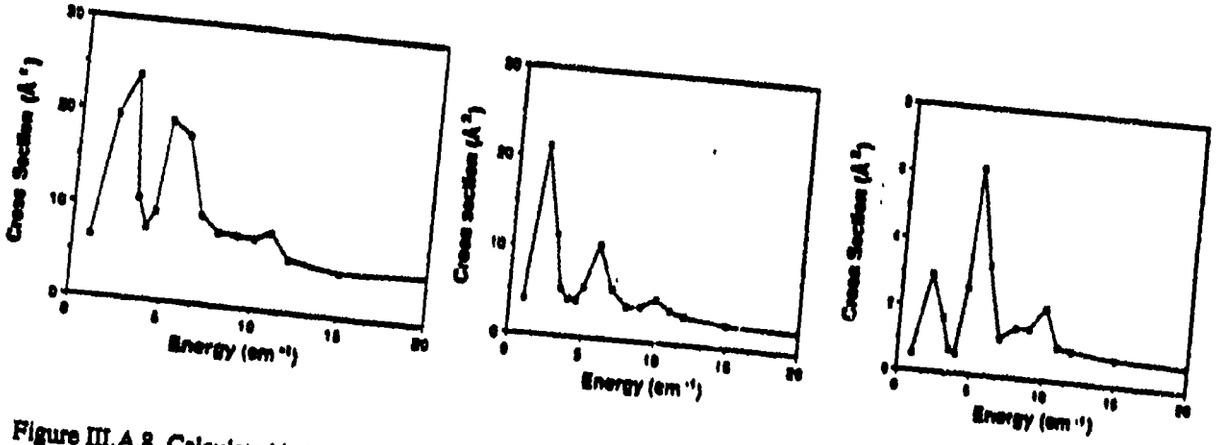

Figure III.A.8 Calculated helium pressure broadening cross sections for (left to right) the $1_{11} - 1_{10}$, $1_{01} - 0_{00}$, and $1_{11} - 0_{00}$ transitions of HDO.

structure in the cross sections that result from the resonant channels. Because of the widely

spaced levels and geometry of this light hydride there is significant variation among these transitions. In addition, these calculations show a continuous monotonic increase in cross section above energies of about 20 cm^{-1}. Of particular interest is the fact that the calculations show that these resonances are spaced widely enough that they survive the thermal averaging to produce significant structure in the pressure broadening cross sections. However, since these calculations were done on a 1 cm^{-1} energy grid, additional calculations will be required to show that no significant resonances were missed. Additional resonances, if present, could smooth out the pressure broadening cross sections by filling gaps.

The calculations on CO - He and HDO - He provide a basis for a qualitative understanding of the experimental results for the other systems for which detailed calculations do not exist. At the lowest temperatures, none of the observed transitions show an increasing cross section with decreasing temperature. Indeed, many show a rapidly decreasing cross section. As would be expected qualitatively, the species with the more widely spaced levels show smaller cross sections, and, within CO, the higher J levels have smaller cross sections. These observations are clearly consistent with the fact that at the lower temperatures the size of the energy defect increases relative to the available translational energy and, therefore, insufficient energy exists to initiate inelastic collisions. However, it is perhaps surprising that there exists only modest state to state variation within CH_3F because the separation of the states of the several observed transitions from their neighbors varies widely. In addition, those species such as CH_3F and CH_2F_2 which have some level spaced $\leq kT$ show cross sections at 4 K considerably higher than at 300 K, presumably due to the existence of the aforementioned resonances.

Finally, it should be noted that the basic question of the asymptotic behavior of cross section in the limit of zero temperature is open. Numerical calculations for the J = 0 - 1 of CO - He indicate a very rapid increase at very low temperatures. Although the J = 0 - 1 experimental data show a significant increase starting at 4 K, the data at the lowest available temperatures appear to be flattening. On the other hand, the calculations for J = 1 - 2 show an initially rapidly rising cross section with decreasing energy, but a flattening at the lowest energy. The theoretical calculations for HDO were done on a coarser energy grid and more uncertainty exists about their low temperature behavior.

Thus, although the general correlation between density of states and behavior of cross section with collision energy may be qualitatively understood, a number of important experiments remain to be done and a special need for additional calculations to strengthen the interplay between experiment and theory exists.

B. Energy Transfer in Polyatomic Molecules

Our work on rotational and fast vibrational energy transfer grew out of an initial interest in constructing models of the internal dynamics of FIR molecular lasers which would include modern ideas of molecular collision dynamics. Although the number of degrees of freedom in these molecular systems might at first glance seem discouraging, we used mm/submm spectroscopic diagnostic techniques to establish *experimentally* the existence of pools of levels which are in equilibrium with each other, thereby substantially simplifying the resulting models. Because of the very high sensitivity of mm/submm spectroscopy to nonthermal rotational populations, this could be done with considerable certainty. Examples of such thermal pools include the equilibria of the vibrational bending modes with the R/T temperature in the HCN discharge FIR laser; all of the J rotational levels within the unpumped K = 1 state of the $^{12}CH_3F$ OPFIR laser; all of the rotational levels within the unpumped symmetry species of the $^{13}CH_3F$ OPFIR, etc.[26,7,27] This work has provided a quantitative model of the complex HCN discharge laser system as well as significant advances in our understanding of OPFIR lasers. Perhaps the most interesting practical result of this latter work was the demonstration and theoretical explanation of the operation of an OPFIR laser in a high pressure, small cavity regime that was previously thought to be forbidden on rather fundamental grounds.[28]

This work is related to other efforts in collisional energy transfer. A number of years ago Oka reviewed collision induced rotational relaxation[29] and reported on his pioneering work as well as on the results of others.[30-33] That work laid out basic 'selection' and 'propensity' rules for rotational collisional energy transfer and presented experimental verification for some of these, especially for those based on spin statistics. Since then, other workers have reported observations of infrared-microwave (ir-mw) double resonance effects.[34-36] Recently, a number of double resonance techniques have been used for quantitative studies of rotational relaxation in polyatomic molecules.[37-42]

From all of this, it has become clear that vibrational energy transfer and rotational energy transfer are not separate and factorable subjects. This is especially true either when systems have very fast vibrational processes which are therefore convolved with rotational processes or when Coriolis or other mixings give rotation like character to 'vibrational' transitions. A nice example of the latter is the work on isotopes of formaldehyde by Haub and Orr.[40] In another example, we have shown in a quantitative modeling of the HCN FIR discharge laser that a similar Coriolis interaction is the principal dissipative agent for the vibrational state containing the upper laser level.[26]

In the work described below time resolved mm/submm-ir double resonance methods were used to obtain the experimental data which formed the basis for the development of nu-

merical models which characterize the molecular energy transfer. The experimental details as well as the results of these investigations have been published in a number of papers.[7,8,27,43] A brief discussion of the diagnostic techniques used for these investigations is included in Appendix B.

1. Modeling: As a first goal in our modeling of FIR lasers and rotational and vibrational energy transfer, we have sought to build the kinds of energy transfer models discussed above that describe the systems in terms of a finite number of individual energy levels and thermal pools along with the energy transfer rates that connect them together. Although the resulting models are too complex for analytical solution, we have found that they may be implemented numerically on microcomputers using relatively simple techniques. In this form nonlinear least squares techniques are used to adjust the rates of the model to match the time resolved data obtained from our experiments. At a more fundamental level we have sought to obtain rates that can be related to fundamental physical processes.

As an example, Fig. III.B.1 illustrates the relevant energy levels and pumps for $^{12}CH_3F$ and $^{13}CH_3F$. Even though vibrational relaxation to the ground state and rotational relaxation of the 'hole' pumped in the lower vibrational state are important processes, they are essentially mirror images of processes in the excited states and for simplicity are not included in the figure. Although spectroscopically these isotopes are very similar, it is important to note

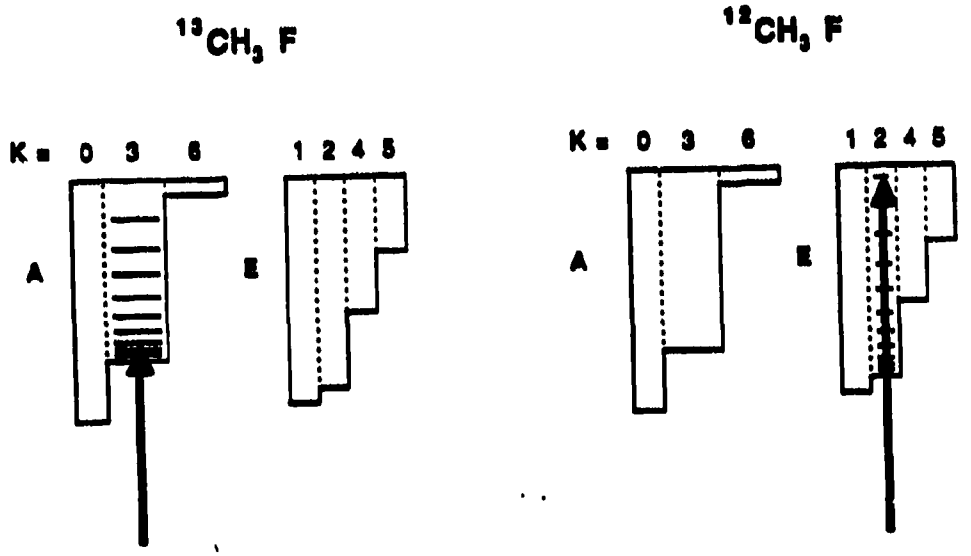

Figure III.B.1 A comparison of the symmetry species, thermal pools, and nonthermal J states within the pumped K manifold for $^{12}CH_3F$ and $^{13}CH_3F$. Areas are representative of the sizes of the partition function of each.

that the CO_2 laser pumps connect rather different J levels and entirely different symmetry

species in the two isotopic species. One measure of the significance of these differences is the rather large difference in their characteristics as FIR lasers.[44] As a result the dynamical data obtained from the time resolved mm/submm-ir double resonance experiments on each species are not strongly correlated.

Briefly, we have found it possible to account for a large and diversified body of experimental data by:

(a) Collecting all of the rotational states of the symmetry species which does not contain the pumped transition into a single thermal pool, with the relative population of the levels within the pool determined by the Boltzmann factor and with the total population free to vary in the model.

(b) Collecting all of the rotational states of the symmetry species which does contain the pumped transition into a similar pool, with the exception of the J states in the pumped K manifold which can have an excess 'nonthermal' population.

(c) Within the pumped K manifold, the nonthermal populations of all J are treated as independent variables.

(d) Additional pools for population transfer to vibrational states are included as required by the magnitude of the vibrational excitation. Typically, for the time resolved mm/submm-ir measurements of energy transfer rates, only the ν_6 is required in addition to the ground vibrational state and the directly pumped ν_3.[7,8] However, for strongly pumped cw laser systems we have found that population transfer to many additional states profoundly affects the laser operation.[28]

The principal energy transfer processes among these pools and states are:

(a) The $\Delta J = n$, $\Delta K = 0$ processes; the fastest of which is the electric dipole allowed $\Delta J = 1$.

(b) The spin statistic allowed $\Delta K = 3n$ processes, which distribute any nonequilibrium population according to a thermal distribution to all other rotational states of the same symmetry.

(c) A vibrational swap processes which, for example, *effectively* transfer population between the A and E symmetry species of the pumped excited vibrational state.

(d) Fast vibrational processes (e. g. $\nu_3 \rightarrow \nu_6$ or $\nu_3 + \nu_3 \rightarrow 2\nu_3$).

(e) Vibrational relaxation resulting from wall collisions.

2. Results: Figures III.B.2 and III.B.3 show examples of observed experimental results from the time resolved mm/submm-ir experiment. Figure III.B.2 shows the very early time emission/absorption associated with the nonthermal population within the K manifold which contains the pumped level (for the case of $^{12}CH_3F$, the K = 2). This early time emission is subsequently followed by rotational relaxation which thermalizes the J states within the K

manifold, causing the subsequent absorption maximum seen in all of the traces. Finally, the excess population in this K manifold is relaxed by transfer to other K states of the same symmetry, via vibrational swapping to the other symmetry species, by vibrational transfer to

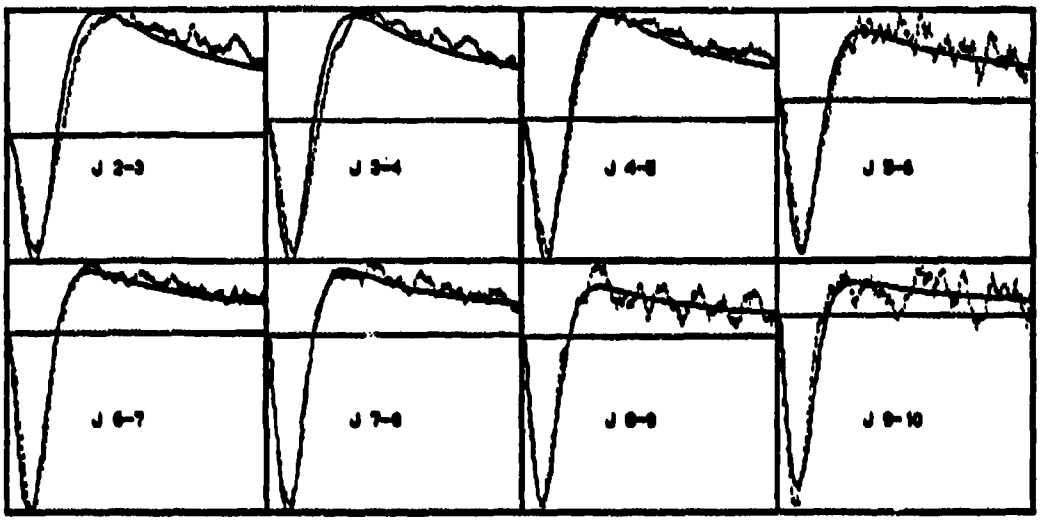

Figure III.B.2 Time resolved response of rotational transitions within the pumped K manifold for $^{12}CH_3F$.

other vibrational states, and ultimately back to the ground vibrational state. Figure III.B.3(upper) shows the arrival (due to the $\Delta K = 3n$ process) of this population in another K state of the same symmetry, and Fig. III.B.3(lower) shows the arrival (due to the vibrational swapping mechanism) of the excitation in a state of the other symmetry of $^{13}CH_3F$.

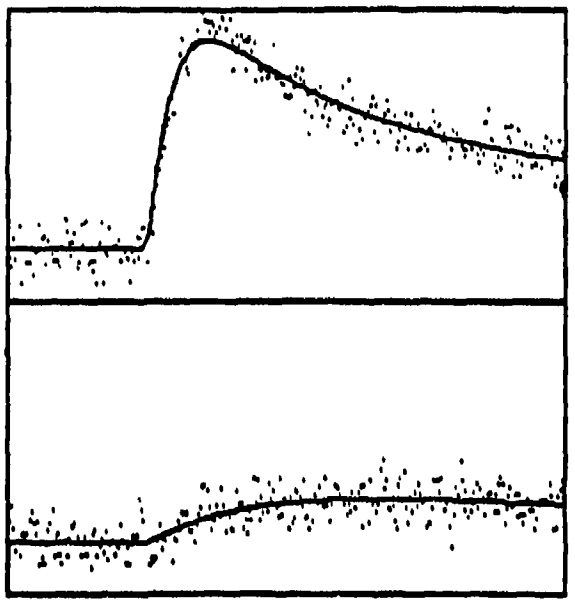

Figure III.B.3 Time response due to the $\Delta K = 3n$ (upper trace) and vibrational swap (lower trace) processes.

Although the details of the states and pools are different, the results are largely independent of isotopic species after effects due to statistical weights, etc. are removed.

The time resolved experimental results shown above were fitted via a nonlinear least squares fit to the parameters shown in Table III.B.1. It can be seen that the agreement between the results obtained for the two species is very good as is the fit to the experimental data shown in Figs. III.B.2 and III.B.3. The different range of $\Delta J = n$ rates which was obtained in the two experiments reflects the difference in the quantum number of the pumped levels relative to levels monitored in the experiment. Numerically, the parameters associated with energy transfer among the pools (i. e. the $\Delta K = 3n$ and vibrational swap) are essentially the same (and, in fact, are often constrained to be the same although they are independently obtainable), as should be expected from the similar energy level structure and multipole moments of the two isotopic species. The $\Delta J = n$ rates show similar trends, with the $^{13}CH_3F$ being somewhat faster than the $^{12}CH_3F$. The differences are of the order expected given that the $^{12}CH_3F$ population starts in

Table III.B.1 Collisional Energy Transfer Rates for CH_3F.

Process	Collision Rates[a] $^{12}CH_3F$	$^{13}CH_3F$
$\Delta K = 3n$	20[b]	20
V - Swap	6.6[b]	6.6
$\Delta J = 0,1$	66.3[b]	66.3
$\Delta J = 2$	0.463	1.000
$\Delta J = 3$	0.314	0.511
$\Delta J = 4$	0.220	0.356
$\Delta J = 5$	0.176	0.280
$\Delta J = 6$	0.152	0.201
$\Delta J = 7$	0.130	
$\Delta J = 8$	0.096	
$\Delta J = 9$	0.084	
$\Delta J = 10$	0.062	

[a] Units are msec^{-1} mTorr^{-1}.

[b] These values were fixed in the nonlinear simulation.

J = 12, K = 2 and in $^{13}CH_3F$ in J = 5, K = 3.

It is worthwhile briefly discussing which parts of the observed time resolved responses are most closely related to the calculated parameters. The 'vibrational-swap' process transcends the spin statistic selection rule and *effectively* transfers population in the excited vibrational state from the symmetry species containing the pump to the other symmetry species. A very direct means of observing this rate is to simply measure the rate of population arrival in a pool state of the opposite symmetry, for $^{13}CH_3F$ K = 1 (K = 3 pumped) and for $^{12}CH_3F$ K = 0 (K = 2 pumped). Although the details of this process are not well understood, Mahan[45] (using the results of London[46] and Margenau[47]) has shown that for cases of near resonance the cross sections for vibrational collisional energy transfer can be considerably enhanced by the presence of a large vibrational transition dipole moment such as exists in CH_3F. The related near resonance process ($\Delta E = 18\ cm^{-1}$) $\nu_3 + \nu_3 \rightarrow 2\nu_3$ has a similarly fast rate in CH_3F.[48] A mechanism of this general nature would lead to a rate which would be largely isotope independent. The rates of the $\Delta K = 3n$ processes are also essentially the same for each of the isotopes. Recently, we have done an additional test of the assumption that the $\Delta K = 3n$ process is the same (i. e. thermal) for n = 1, 2, etc. In these experiments $^{12}CH_3F$ was used. K = 2 was pumped, and K = 1, K = 4, and K = 5 were observed. All were found to have the same time response.

The experimental results for the $\Delta J = n$ processes are more complex and interesting. Clearly, in the limit of large energy gap ($\Delta E \geq kT$) the energy gap must play some role in addition to the role played by the size of the change in J. Effects of this type are well known in simple diatomic species although considerable controversy exists about 'energy gap', 'power law', etc. explanations.[49-51] However, in both of the examples here, the energy gap is smaller than kT and it might be reasonably expected that it would induce relatively small differences between the values of the $\Delta J=n$ rates of the two isotopic species. Figure III.B.4 shows a plot of the $\Delta J=n$ rates obtained for each as a function of ΔJ. The similarity of these two sets of

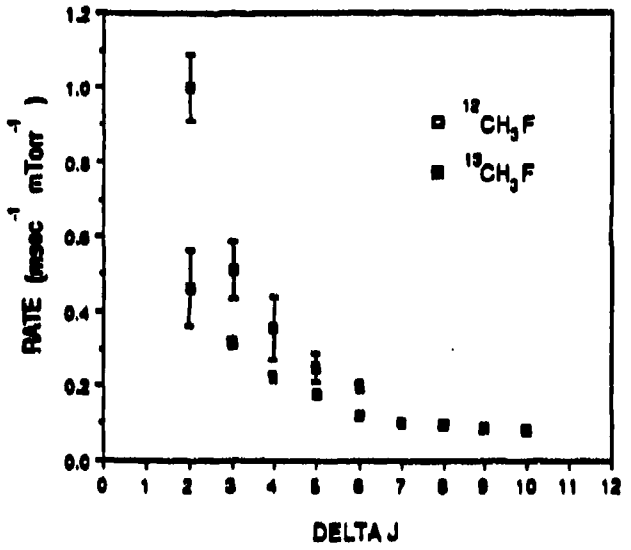

Figure III.B.4 Plot of $\Delta J = n$ rates for $^{12}CH_3F$ and $^{13}CH_3F$.

data seems to indicate that the energy gap and quantum number differences are not too important in the regime of these experiments.

Because the deconvolution of the time resolved responses of these complex systems might appear to be rather complicated and might provide results that are very model dependent, we have also done a number of 'sensitivity' checks on the numerical model. First, it should be recognized that at very early times (i.e. immediately after the Q-switched laser deposits the population in the upper pumped state), first order (i. e. one step) processes dominate. Simple considerations lead to the conclusion that the slope of the absorption at $t = 0$ represents the *difference* between the $\Delta J = n$ rates that populate the upper and lower J levels for transitions within $K = 2$. Careful numerical investigation shows, however, that the definition of early time depends upon the size of n because for large n with fairly slow $\Delta J = n$ rates, faster two step processes can become important at fairly early times. Nevertheless, we have been able to obtain from these early time slopes and simple analytical expressions results that are in good agreement with the results of the numerical models.

In addition, we have carried out a number of numerical investigations of small modifications of the theory (e. g. making the $\Delta J = n$ rates functions of J; making the $\Delta K = 3n$ rates small functions of J, etc.). Although these can make small changes in the details of the fit at medium and long times, these changes are modest and the rates calculated from the fit are largely independent of these choices. Finally, the good agreement between the results obtained from independent analyses of the two isotopic species is good evidence that the rates obtained from the model are, in fact, closely related to the physical processes with which they are identified.

C. Millimeter and Submillimeter Technology

1. A Millimeterwave Quasioptical IMPATT Combiner Source: Conventional waveguide power combiners are limited in power output, efficiency, and number of sources that may be combined in the millimeter wave region. This limitation is a consequence of the requirement that linear dimensions of conventional waveguide resonators be of the order of one wavelength to achieve acceptable mode separation and to avoid multimode operation. On the other hand, quasi-optical resonators have linear dimensions large compared to wavelength and they offer an attractive approach to overcome these limitations. In addition, the Q of such resonators is high, resulting in a pure output frequency spectrum from a quasi-optical millimeter wave power combiner. An experimental investigation of quasi-optical millimeter wave power combiners based upon the theory developed earlier by Mink[52] is discussed in this paper. The approach utilizes an array of source elements placed at the surface of one reflecting surface on an open resonator. For testing purposes, energy is extracted at the other reflector through a conventional waveguide.

To experimentally investigate the feasibility of quasi-optical power combining of millimeter wave sources, an approach which combines a wave beam or Fabry-Perot resonator is used as the combining element and IMPATT (Impact Avalanch Transit Time) diode sources are configured in a rectangular array with each diode connected to a loop coupling element. The cavity configuration is shown in the figure below. For ease of fabrication, a wave beam resonator of circular symmetry is employed in this experiment. The resonator consists of two reflecting surfaces which are large relative to the operating wavelength. One surface is a planar reflector and the other is curved such that it tends to "focus" the electromagnetic energy at the planar reflector.

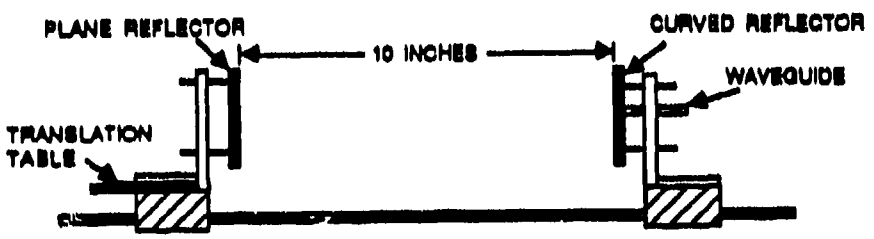

Quasi-optical cavity.

A goal of this experiment was to show that a large number of sources could be combined and that the IMPATT diode sources would cohere with each other in the combiner environment. Also, for this experiment, it was decided to utilize commercially available IMPATT sources (Hughes 60 GHz CW IMPATT). Because such devices are already mounted and since one side of the diode is connected to a heat sink, one could not easily employ the coupling technique of balanced electrical dipoles as discussed by Mink.[52] To achieve efficient coupling with a dense array of elements it was decided that loop coupling could be utilized. Other techniques could have been employed however, but they are not easily extrapolated to a large number of sources. Space limitations here prevent the presentation of the theory of loop coupling which will be published at a later date. Each source is attached to a a small radiating loop as shown in the figure below. The diode heat sink is embedded in a copper rod 1 mm greater in diameter. A filter network is then milled in the copper as well as a slot to permit passage of the loop wire to the diode cap. This assemblage is then embedded in the plane surface of the reflector and biasing current are passed through the filter network and the loop to the diode. The filter network consists of a series of quarter wavelength transmission lines designed to present a low impedance at the point where the loop passes through the ground plane.

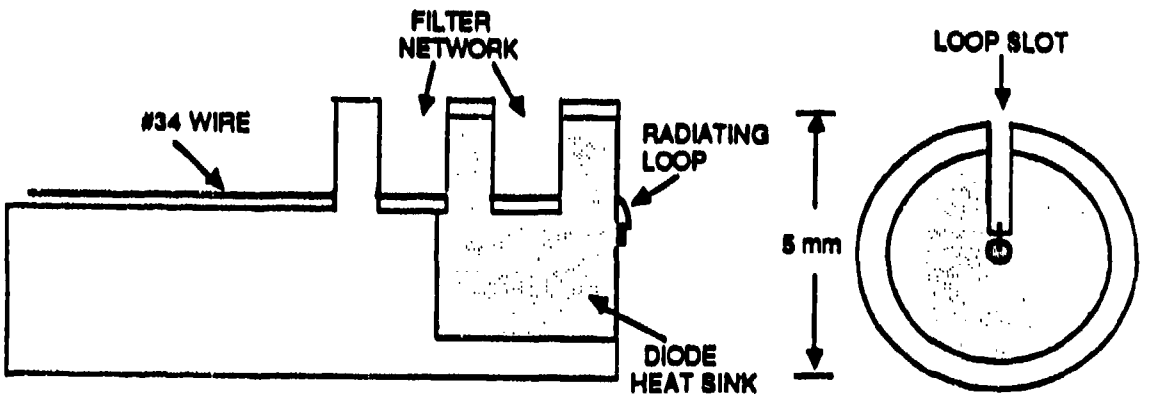

Diode package and rod assembly, side and front view.

Quasi-optical resonators are based upon reiterative wave beams or beam modes. These modes were first described by Goubau and Schwering[53] and for the purposes of this experiment only the lowest order mode is of interest. In the transverse direction the lowest order mode may be expressed by a Gaussian distribution. In directions transverse to the direction of propagation, characteristic dimensions of the fields within the wave beam resonator are much larger than those of a conventional waveguide. They range from about 10 to 100 wavelengths.

As previously mentioned, Hughes 60 GHz CW IMPATT diodes were used to test the theory of quasi-optical power combining. Diodes selected were silicon double drift devices with a doping profile of p^+pnn^+, where the p^+ and n^+ regions allow for ohmic contacts to be made to the external circuit. As commercially packaged, the p^+ region is bonded to metalized diamond which is thermally and electrically conductive. The diamond is then embedded in a 0.3 x 0.4 cm cylindrical copper encasement to serve as a heat sink and mount. The n^+ region is coupled to a gold band and then to a gold button 0.09 cm in diameter sealed to a quartz ring standoff 0.01 cm above the active device as shown below. These packaging dimensions are believed to be critical to the experimental results discussed later. The IMPATT diodes are designed to operate at 250°C with a MTBF of 10,000 hours. At the rated bias current, approximately 7 watts of heat would be dissipated from each diode. The diodes used were certified individually by the manufacturer with the following intrinsic variations: capacitance ~ 1.50 to 1.91 pf; breakdown voltage (minimum voltage for current to flow) ~22.4 to 24.6 volts; bias voltage for rated CW frequency ~26.2 to 29.3 volts; rf power ~210 to 280 mW; rated frequency ~59.0 to 61.6 GHz. Differences in doping concentrations, device thickness, and operating temperature (which induces thermal expansion in the p and n regions) affect the transit time of the electrons and hence the rf frequency for a particular diode.[54]

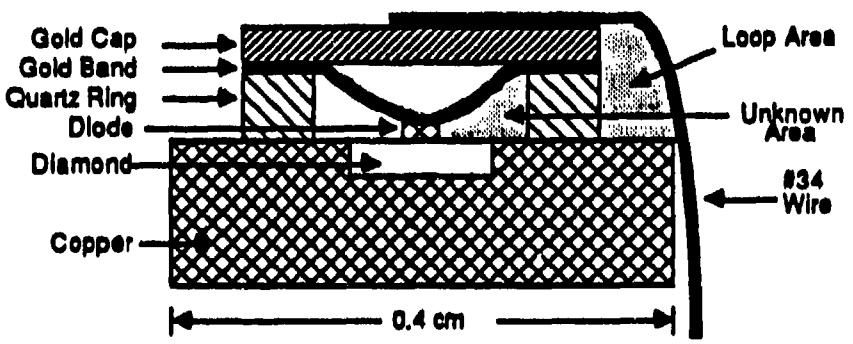

IMPATT diode package configuration with coupling loop, adapted from Kuno.[4]

The combiner design allowed for 21 diode rod assemblies spaced 9.2 mm center to center in a modified rectangular pattern. Each rod was embedded in a 4x4x0.5 inch copper plate, as shown below. The plate served as the cavity plane reflector and an effective heat sink. The diode spacing was taken from Mink[52], which gives normalized source spacing with respect to fractional mode power and driving point resistances for various array sizes. He concluded that efficient coupling could be expected in the transverse fundamental mode when the diodes were properly spaced. The ultimate goal is to combine many individual diodes to obtain one high power source. Theory predicts that if a single diode couples 1 mW of rf power into the fundamental mode of a quasi-optical power combiner, then, with diode spacing and cavity dimensions held constant, a 5x5 array of diodes would combine to yield 300 mW, a 7x7 array - 630 mW, and a 9x9 array - 800 mW. This is satisfying on physical grounds because in the limit of few diodes their "antenna patterns" excite many modes in addition to the one coupled into the output waveguide. As the diode array begins to fill the spot size of the mode at the plane reflector, its "antenna pattern" is then coupled primarily into a single mode. Finally, as the array becomes larger than the spot size, the power radiated by the outer diodes is lost.

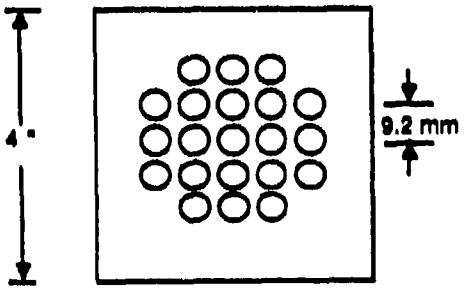

Planar reflector with embedded diode assemblages.

The manufacturer calibrated each diode in a standard IMPATT diode test circuit in which a diode in reduced-height waveguide is current biased and rf exits to full-height waveguide through a stepped transition section. Such a test circuit was obtained and a sample diode was found to operate at its certified operating point discussed earlier. These sources operate in a low Q mode and do not exhibit high spectral purity. Power is typically distributed across a bandwidth of several hundred kHz or more. Conversely, a quasi-optical cavity will provide a significantly higher Q. Since the spectral purity of an oscillator is related to the Q of its resonant circuit, the possibility of significantly enhanced spectral purity exists. This could be dramatically observed by changing the cavity spacing so that the Q of the modes varied. More than an order of magnitude variations in spectral purity occurred

and, in favorable cases, HWHM (half width at half maximum) bandwidths that approached 10 kHz were observed.

For a desired operating frequency of 60 GHz, the coupling loop area was calculated to 0.4 mm^2. Teflon and enamel coated 30 to 40 gauge copper wire was tested. The diode was current biased over the complete range up to 300 milliamps. This produced rf between 40 and 45 GHz. Detectable oscillations could not be found above 45 GHz regardless of bias. Bias current ranged from 90 to 150 milliamps when rf was detected, half the nominal current for 60 GHz operation. Output power was disappointingly low. The frequency/current relationship in the 40 to 45 GHz range at these low bias currents was distinctly linear, an interesting but not a useful result for this experiment.

The disparity between calculated and observed oscillation frequency for the 0.4 mm^2 loop area is theorized to be a result of the packaging dimensions and the bias filter network. The figure above shows that beneath the gold cap is an area in which a gold band bridges the length of the quartz ring connecting the cap to the n^+ diode region. Furthermore, the band orientation beneath the cap is unknown. This unexposed area may contribute additionally to the 0.4 mm^2loop area constructed externally to the cap and is loaded with dialectrics. Accordingly, the loop slot was milled down close to the cap to reduce the total loop area. Better impedance matching and increased radiated power were anticipated.

The results were encouraging. It was possible to achieve an order of magnitude greater output power at bias currents above 200 milliamps at a specific frequency. Lost, however, were the broad tunability characteristics previously found with larger loops and lower currents. Rather, the diode was tunable over a 700 to 800 MHz range for bias currents between 200 and 270 milliamps. It was difficult, though possible, to achieve operating frequencies as high as 42 GHz. This necessitated pressing the wire loop around the diode cap to get the smallest external loop area. Possibly owing to the variability of the unknown area beneath the cap, most diodes more easily produced a radiation in the 33 to 37 GHz range. Refinements to the loop area would produce output near 35 GHz for most diodes. Number 34 gauge enamel coated wire yielded the best performance for both output power and durability. With a Hewlett-Packard 8555 spectrum analyzer, high spectral purity was observed even when the cavity length was reduced to a few inches. At the designed length of 10 inches, the loaded cavity Q was measured to be 5000. For a single oscillating diode in this configuration, spectral purity was measured at 50 kHz HWHM bandwidth.

Frequency, bias current, and loop area were defined for several diodes and the quest to phase couple two and more diodes in the cavity was launched. Ka band (26.5 - 40 GHz) waveguide replaced the V band waveguide to accomodate the newly selected 35 GHz region of operation. A wavemeter, crystal detector, oscilloscope, and spectrum analyzer were

connected to measure the frequency and power of the diode. Two diodes were selected and their loop areas were adjusted for operations near 35 GHz. When within 1 GHz of each other, they became candidates for coupling in the combiner. Coupling with two diodes was not spontaneous, but easily achieved by alternately adjusting the bias current and cavity length. Precise current tuning was achieved with precision potentiometers. Cavity lenth was adjusted with a micrometer-driven translation table on which the plane reflector was mounted. The activity was easily monitored from either the dc level on the scope or on the spectrum analyzer. Once the diodes were coupled, the spectrum analyzer revealed that they remained so despite varying bias current by as much as 5%. Coupling enhanced spectral purity which was measured to be 25 kHz HWHM bandwidth. In combination, two diodes produced about four times more power than the individual diodes, in agreement with theoretical predictions. A third diode was prepared in a similar fashion and bias tuned to near the operating frequency of the first two diodes. Phase locking of this third diode was straight forward. It is expected that the rest of the array can be filled in by continuing this process.

In conclusion, power combining with millimeter wave IMPATT diodes in a quasi-optical cavity has been demonstrated. Power exceeding merely the sum of the individual diode outputs has been observed as predicted. The diodes oscillating in a high Q quasi-optical cavity produce radiation of high spectral purity. Formidable obstacles still exist in understanding impedance matching of wire loop coupled antennas to IMPATT diodes. Inherent variability in commercially packaged IMPATT diodes has complicated the theoretical calculation of oscillating frequencies due to the introduction of unknown coupling loop geometries. These problem areas may eventually be overcome by epitaxially growing diodes on a single substrate and fabricating coupling loops to precise dimensions with microstrip techniques to produce a large array of millimeter wave diodes in a monolithic integrated circuit.

2. Submillimeterwave Imaging: We have also carried out at a modest level a submillimeterwave passive imaging project. The impetus for this work has been our interest in the development of very sensitive broadband detector techniques for this spectral region. Since these detectors are the key to passive imaging in this spectral region, several observations were made both within the laboratory and in the external environment. These used small (4" - 8") optics and slow scan techniques. Orders of magnitude enhancements would result from the use of larger antennas and focal plan arrays. One of the most remarkable results from this work was that when we presented our results at an ARO sponsered workshop on millimeter and submillimeter wave imaging, the group in attendance concluded that they were the only submillimeter wave images that had ever been produced!

In the selection of an active or passive imaging system, basic physical considerations impose a strong wavelength bias. At long wavelengths active systems (e. g. radar) are ordinarily selected, while at short wavelengths passive systems are predominant (e. g. eyesight, film, thermal sensors, etc.). This is largely due to the fact that thermal emission falls rapidly at long wavelength, peaking at 10μ for objects of ~300 K and at ~6000 Å for objects illuminated by the sun.

Our work was based on theoretical and experimental results which showed that many of the useful features of passive imaging at short wavelengths can also be realized at much longer wavelengths (300μ - 3000μ) by the use of appropriate detector technology and that systems based on these longer wavelengths have a number of unique and useful properties including, but not limited to:

(1) Much improved penetration of clouds, fog, smoke.
(2) Different target signatures.
(3) Much less well developed countermeasures.

The signal to noise ratio of a broadband thermal detector is given by

$$S/N = [P_s/NEP]\,[\Delta t]^{1/2}$$

where P_s is the power incident on the detector, NEP the noise equivalent power of the detector, and Δt the integration time. In the mm/submm spectral region it is ordinarily a good approximation to assume that the Rayleigh-Jeans limit applies and that the signal power from the target (assumed here for simplicity to be a black body) is given by

$$P_s = 2kT_s\Delta\nu$$

where k is Boltzmann's constant, $\Delta\nu$ is the bandwidth of the detector, and T_s the temperature of the target. The resulting signal to noise ratio is[55]

$$S/N = \frac{2kT_s \Delta\nu \sqrt{\Delta t}}{NEP}$$

For T_s = 300 K, $\Delta\nu$ = 10 GHz, Δt = 10 msec, and NEP = 10^{-15} W/Hz$^{-1/2}$, a S/N ~ 10^4 is calculated. This number would be reduced for emissivities < 1, temperatures < 300 K, but would be increased by bandwidths > 10 GHz. In any event, it is a large number and attests to the basic sensitivity of broadband detectors at long wavelength. Thus, we conclude that state-of-the-art thermal detectors operating in the mm/submm can detect small temperature differences with moderate time constants.

A laboratory demonstration of this was reported[56] at the 12th International Conference on Infrared and Millimeter Waves. The figure below shows a representative image of a man with glasses. This was made using a raster scanned system with a 30 msec time constant, a bandwidth from ~100 -1000 GHz, a detector NEP of ~10^{-15} W/Hz$^{1/2}$ and an 8" mirror. The dynamic range and signal to noise of the image vastly exceed the grey scale capabilities of the display shown.

Participating Scientific Personnel

1. Frank C. De Lucia, Professor of Physics
2. Eric Herbst, Professor of Physics
3. Paul Helminger, Professor of Physics, University of South Alabama
4. D. D. Skatrud, Assistant Professor (adjunct)
5. J. W. Mink, Senior Reserach Scientist
6. Major Kevin Cogan, Army DARP Fellow
7. S. H. Shostak, Research Associate
8. W. L. Ebenstein, Research Associate
9. Rodney McCormick, Graduate Student (Ph. D. 1987)
10. Richard Crownover, Graduate Student
11. Dan Wiley, Graduate Student
12. Todd Anderson, Graduate Student
13. Henry Everitt, Graduate Student
14. Tom Goyette, Graduate Student

V. BIBLIOGRAPHY

1. W. C. King and W. Gordy, Phys. Rev. **90**, 3139 (1953).
2. P. Helminger, F. C. De Lucia, and W. Gordy, Phys. Rev. Lett. **25**, 1397 (1970).
3. P. Helminger, J. K. Messer, and F. C. De Lucia, Appl. Phys. Lett. **42**, 309 (1983).
4. R. A. Booker, R. L. Crownover, F. C. De Lucia, J. Mol. Spectrosc. **128** , 62 (1988).
5. D. R. Willey, R. L. Crownover, D. N. Bittner, F. C. De Lucia, J. Chem. Phys. **89**, 1923 (1988).
6. D. R. Willey, D. N. Bittner, and F. C. De Lucia, J. Mol. Spectrosc. **133**, 182 (1989).
7. R. I. McCormick, H. O. Everitt, F. C. De Lucia, and D. D. Skatrud, IEEE J. Quant. Electron. **QE-23**, 2069 (1987).
8. R. I. McCormick, F. C. De Lucia, and D. D. Skatrud, IEEE J. Quant. Electron., **QE-23**, 2060 (1987).
9. J. K. Messer and F. C. De Lucia, Phys. Rev. Lett. **53**, 2555 (1984).
10. D. R. Willey, R. L. Crownover, D. N. Bittner, and F. C. De Lucia, J. Chem. Phys. **89**, 6147 (1988).
11. D. R. Willey, D. N. Bittner, and F. C. De Lucia, J. Mol. Spectrosoc. **134** , 240 (1989).
12. D. R. Willey, D. N. Bittner, and F. C. De Lucia, Mol. Phys. **66**, 1 (1988).
13. D. R. Willey, T. M. Goyette, W. L. Ebenstein, and D. N. Bittner, J. Chem. Phys., in press.
14. D. N. Travis, J. C. McGurk, D. McKeown, R. G. Denning, Chem Phys. Lett. **45**, 287 (1977).
15. P. B. Davies and A. J. Morton-Jones, Appl. Phys. **B42**, 35 (1987).
16. T. A. Brunner and D. Pritchard, Ad. Chem. Phys. **50**, 589 (1982).
17. E. H. Putley, Infrared Physics **4**, 1 (1964).
18. R. D. Levine, B. R. Johnson, J. T. Muckerman, and R. B. Bernstein, J. Chem. Phys. **49**, 56 (1968).
19. W. Erlewein, M. von Seggern, and J. P. Toennies, Z. Physik **211**, 35 (1968).
20. M. von Seggern and J. P. Toennies, Z. Physik. **218**, 341 (1969).
21. A. Palma and S. Green, J. Chem. Phys. **85**, 1333 (1986).
22. R. B. Nerf, Jr., and M. A. Sonnenberg, J. Mol. Spectrsoc. **58**, 474 (1975).
23. S. Green and L. D. Thomas, J. Chem. Phys. **73**, 5391 (1980).
24. S. Green, J. Chem. Phys. **82**, 4548 (1985).
25. S. Green, private communication.
26. D. D. Skatrud and F. C. De Lucia, Appl. Phys. Lett. **46**, 631 (1985).
27. H. O. Everitt and F. C. De Lucia, J. Chem. Phys. **90**, 3520 (1989).
28. H. O. Everitt, D. D. Skatrud, and F. C. De Lucia, Appl. Phys. Lett. **49**, 16 (1986).
29. T. Oka, in *Ad. in At. Mol. Phys.* **9**, 127, Academic Press, New York, 1973.
30. A. P. Cox, G. W. Flynn, and E. B. Wilson, Jr., J. Chem. Phys. **46**, 3262 (1967).
31. A. M. Ronn and E. B. Wilson, Jr. J. Chem. Phys. **46**, 3262 (1967).
32. L. Frenkel, H. Marantz, and T. Sullivan, Phys. Rev. **A3**, 1640 (1971).
33. P. J. Seibt, J. Chem. Phys. **57**, 1343 (1972).
34. H. Jetter, E. F. Pearson, C. L. Norris, J. C. McGurk, and W. H. Flygare, J. Chem. Phys. **59**, 1796(1973).
35. S. Kano, T. Amano, and T. Shimizu, J. Chem. Phys. **64**, 4711 (1976).
36. W. A. Kreiner, A. Ever, and H. Jones, J. Mol. Spectrosc. **52**, 420 (1974).
37. E. N. Chesnokov and V. N. Panfilov, Sov. Phys. JETP **46**, 1112 (1977).

38. L. Laux, B. Foy, D. Harradine, and J. I. Steinfeld, J. Chem. Phys. **80**, 3499 (1984).
39. D. Harradine, B. Foy, L. Laux, M. Dubs, and J. I. Steinfeld, J. Chem. Phys. **81**, 4267 (1984).
40. J. G. Haub and B. J. Orr, J. Chem. Phys. **86**, 3380 (1987).
41. F. Menard-Bourcin and L. Doyennette, J. Chem. Phys. **88**, 5506 (1988).
42. B. Foy, J. Hetzler, G. Millot, and J. I. Steinfeld, J. Chem. Phys. **88**, 6838 (1988).
43. W. H. Matteson and F. C. De Lucia, IEEE J. Quant. Electron. **QE-19**, 1284 (1983).
44. *Review of Infrared and Millimeter Waves* **2**, K. Button, M. Inguscio, and F. Strumia, eds.,Plenum, New York, (1984).
45. B. H. Mahan, J. Chem. Phys. **46**, 98 (1967).
46. F. London, Z. Phys. **63**, 245 (1930).
47. H. Margenau, Rev. Mod. Phys. **11**, 1 (1939).
48. R. S. Sheorey and G. W. Flynn, J. Chem. Phys. **72**, 1175 (1980).
49. R. D. Levine, Ann. Rev. Phys. Chem. **29**, 59 (1978).
50. M. H. Alexander, E. F. Jendrek, P. J. Dagdigian, J. Chem. Phys. **73**, 3797(1980).
51. T. A. Brunner, R. D. Driver, N. Smith, and D. E. Pritchard, Phys. Rev. Lett. **41**, 856 (1978).
52. J. W. Mink, IEEE Transactions on Microwave Theory and Techniques **MTT-34** (1986).
53. G. Goubau and F. Schwering, IRE Trans. Antennas Propagat. **AP-9**, 248 (1961).
54. H. J. Kuno, Infrared and millimeter waves **1**, K. J. Button, Ed. New York: Academic Press, 1979, pp. 55-128.
55. T. G. Phillips, Proceedings of Summer School on Millimeter and Submillimeter Astronomy, Stirling Scotland, June(1987).
56. D. N. Bittner, R. L. Crownover, F. C. De Lucia, and S. L. Shostak, 12th International Conference on Infrared and Millimeter Waves, Miami, 1987.